# FAMU: study of the energy dependent transfer rate $\Lambda_{\mu p \to \mu O}$

IOP Conf. Series: Journal of Physics: Conf. Series **1138** (2018) 012017 doi:10.1088/1742-6596/1138/1/012017

# FAMU: study of the energy dependent transfer rate $\Lambda_{\mu p \to \mu O}$

**E Mocchiutti[1], V Bonvicini[1], M Danailov[1,2], E Furlanetto[1,3], K S Gadedjisso-Tossou[1,4,5], D Guffanti[1,6], C Pizzolotto[1], A Rachevski[1], L Stoychev[1,4], E Vallazza[1], G Zampa[1], J Niemela[4], K Ishida[7], A Adamczak[8], G Baccolo[9,10], R Benocci[9,11], R Bertoni[9], M Bonesini[9], F Chignoli[9], M Clemenza[9,10], A Curioni[9], V Maggi[9,11], R Mazza[10], M Moretti[9,10], M Nastasi[9,10], E Previtali[9], D Bakalov[12], P Danev[12], M Stoilov[12], G Baldazzi[13,14], R Campana[13], I D'Antone[13], M Furini[13], F Fuschino[13,15], C Labanti[13,15], A Margotti[13], S Meneghini[13], G Morgante[13,15], L P Rignanese[13,14], P L Rossi[13], M Zuffa[13], T Cervi[16,17], A De Bari[16,17], A Menegolli[16,17], C De Vecchi[17], R Nardò[17], M Rossella[17], A Tomaselli[17,18], L Colace[19,20], M De Vincenzi[19,21], A Iaciofano[19], F Somma[19,22], L Tortora[19], R Ramponi[23], A Vacchi[1,3,7]**

[1] National Institute for Nuclear Physics (INFN), Sezione di Trieste, via A. Valerio 2, 34127 Trieste, Italy
[2] Elettra-Sincrotrone Trieste S.C.p.A., SS14, Km 163.5, 34149 Basovizza, Trieste, Italy
[3] Mathematics and Informatics Department, Udine University, via delle Scienze 206, Udine, Italy
[4] The Abdus Salam International Centre for Theoretical Physics, Strada Costiera 11, Trieste, Italy
[5] Laboratoire de Physique des Composants à Semi-conducteurs (LPCS), Département de physique, Université de Lomé, 01 BP 1515 Lomé, Togo
[6] Gran Sasso Science Institute - INFN-LNGS, via F. Crispi 7, L'Aquila, Italy
[7] RIKEN-RAL RIKEN Nishina Center for Accelerator-Based Science, 2-1, Hirosawa, Wako, Saitama 351-0198, Japan
[8] Institute of Nuclear Physics, Polish Academy of Sciences, Radzikowskiego 152, PL31342 Kraków, Poland
[9] National Institute for Nuclear Physics (INFN), Sezione di Milano Bicocca, piazza della Scienza 3, Milano, Italy
[10] Università di Milano Bicocca, Dip. di Fisica "G. Occhialini", piazza della Scienza 3, Milano, Italy
[11] Università di Milano Bicocca, Dip. di Scienze dell'Ambiente e della Terra, piazza della Scienza 1, Miano, Italy
[12] Institute for Nuclear Research and Nuclear Energy, Bulgarian Academy of Sciences, blvd. Tsarigradsko ch. 72, Sofia 1142, Bulgaria
[13] National Institute for Nuclear Physics (INFN), Sezione di Bologna, viale Berti Pichat, 6/2, Bologna, Italy
[14] Department of Physics and Astronomy, University of Bologna, viale Berti Pichat, 6/2, Bologna, Italy
[15] INAF-IAFS Bologna, Area della Ricerca, via P. Gobetti 101, Bologna, Italy
[16] Department of Physics, University of Pavia, via Bassi 6, Pavia, Italy
[17] National Institute for Nuclear Physics (INFN), Sezione di Pavia, via Bassi 6, Pavia, Italy

[18] Department of Electrical, Computer, and Biomedical Engineering, University of Pavia, via Ferrata 5, Pavia, Italy
[19] National Institute for Nuclear Physics (INFN), Sezione di Roma Tre, via della Vasca Navale 84, Roma, Italy
[20] Dipartimento di Ingegneria Università degli Studi Roma Tre, via V. Volterra, 62, Roma, Italy
[21] Dipartimento di Matematica e Fisica, Università di Roma Tre, via della Vasca Navale 84, Roma, Italy
[22] Dipartimento di Scienze, Università di Roma Tre, viale G. Marconi 446, Roma, Italy
[23] IFN-CNR, Department of Physics - Politecnico di Milano and National Institute for Nuclear Physics (INFN), Sezione di Milano Politecnico, piazza Leonardo da Vinci 32, 20133 Milano, Italy

E-mail: Emiliano.Mocchiutti@ts.infn.it

**Abstract.** The main goal of the FAMU experiment is the measurement of the hyperfine splitting (hfs) in the 1S state of muonic hydrogen $\Delta E_{hfs}(\mu^- p)1S$. The physical process behind this experiment is the following: $\mu p$ are formed in a mixture of hydrogen and a higher-Z gas. When absorbing a photon at resonance-energy $\Delta E_{hfs} \approx 0.182$ eV, in subsequent collisions with the surrounding $H_2$ molecules, the $\mu p$ is quickly de-excited and accelerated by $\sim 2/3$ of the excitation energy. The observable is the time distribution of the K-lines X-rays emitted from the $\mu Z$ formed by muon transfer $(\mu p) + Z \rightarrow (\mu Z)^* + p$, a reaction whose rate depends on the $\mu p$ kinetic energy. The maximal response, to the tuned laser wavelength, of the time distribution of X-ray from K-lines of the $(\mu Z)^*$ cascade indicate the resonance. During the preparatory phase of the FAMU experiment, several measurements have been performed both to validate the methodology and to prepare the best configuration of target and detectors for the spectroscopic measurement. We present here the crucial study of the energy dependence of the transfer rate from muonic hydrogen to oxygen ($\Lambda_{\mu p \rightarrow \mu O}$), precisely measured for the first time.

## 1. Introduction

FAMU (Fisica degli Atomi Muonici) is a high precision spectroscopy experiment, conceived to exploit exotic atoms properties to study and test the quantum electro-dynamics (QED).

The main goal of the FAMU experiment is to measure for the first time the hyperfine splitting of the $\mu p$ ground state. Through the measurement of the hyperfine splitting of the $\mu p$ ground state it is possible to determine the proton Zemach radius. In literature, the "standard" measurement of the Zemach radius of the proton $R_p$ is achieved using ordinary hydrogen. A comparison with the value extracted from muonic hydrogen may reinforce or delimit the proton radius puzzle [1].

Muonic hydrogen atoms ($\mu p$) are formed in a hydrogen gas target. In subsequent collisions with $H_2$ molecules, the $\mu p$ de-excite to the thermalized $\mu p$ in the ground state ($(1S)_{F=0}$). At this point, a variable frequency mid infrared laser light is used to illuminate the gas target. When the frequency is tuned on the hyperfine splitting resonance, singlet-to-triplet transitions are induced. A spontaneous radiative de-excitation of the $(1S)_{F=1}$ state of $\mu p$ atoms has a very low probability and thus collisions with neighboring molecules establish an effective mechanism of spin-flip de-excitation [2]. These collisions are non-radiative processes so that photons are not observed. Due to momentum conservation, the transition energy is partially converted to kinetic energy that sum up to the thermal kinetic energy of the $\mu p$ system. The $\mu p$ atom in this status is called "epithermal" $\mu p$. The average kinetic energy acquired by the $\mu p$ is about two-thirds of the hyperfine transition energy ($\approx 120$ meV).

In the FAMU experiment the energy dependence of the muon transfer from muonic hydrogen to another higher-Z gas is exploited to detect the occurred transition in $\mu p$. In general, the

muon-transfer rate at low energies $\Lambda_{\mu p \to \mu Z}$ is energy independent. However, for a few gases this is not true. For example, it was found that oxygen exhibits a peak in the muon transfer rate $\Lambda_{\mu p \to \mu O}$ (in the following we use the abbreviate form "$\Lambda_{pO}$") at the epithermal energy [3].

The transfer to a heavier atom, $\mu^- p + {}^A Z \to (\mu^- {}^A Z)^* + p$, leaves the muon into high orbital states of the newly produced muonic atom $(\mu^- {}^A Z)^*$. The muon atomic orbit equivalent to the electron $K$ orbit has a principal quantum number $n_\mu \approx (m_\mu/m_e)^{(1/2)} \approx 14$ and it is reached by the muon in a few femtoseconds from the instant of its atomic capture [4]. The muon cascades down rapidly to the lowest quantum state available, $1S$. In the case of light elements, de-excitation starts with Auger process until the quantum number reaches values from 3 to 6 at which radiative transitions take over. During radiative transitions, X-rays are emitted at an energy corresponding to the energy levels difference. In the oxygen case, these radiative transitions have energies of the order of ≈100 keV and are easily detectable.

Thus, by adding small quantities of oxygen to hydrogen, one can observe the number of hyperfine transitions, which take place from the muon-transfer events, by measuring the time distribution of the characteristic X-rays of the added gas.

In order to fully exploit this effect, the energy dependence of the muon transfer rate from muonic hydrogen to oxygen must be precisely determined. This measurement was performed as a preparatory step of the FAMU experiment. Details of the data analysis concerning the muons transfer rate measurement are reported in this paper.

## 2. Apparatus setup

The setup of this FAMU data taking, performed in 2016, is described in details in [5]. A beam hodoscope was placed in front of a high pressure gas contained in a thermalized aluminium vessel, surrounded by X-rays detectors. Figure 1, left panel, shows a CAD drawing of the

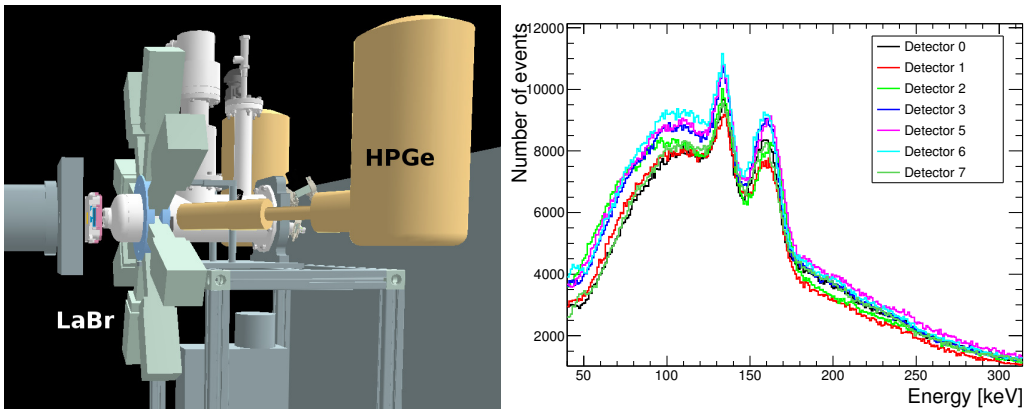


**Figure 1.** Left panel: CAD drawing of the FAMU experimental setup. The star with eight $LaBr_3(Ce)$ detectors is shown together with two HPGes. Muons entered the target from the left side of the figure. Right panel: energy spectrum of each $LaBr_3(Ce)$ detector for delayed events. The $K_\alpha$(133 keV) and the $K_\beta$(158 keV) + $K_\gamma$(167 keV) lines can be observed.

experimental setup. Muons enter the target from the left side (where the beam pipe tube is shown). The FAMU experimental method requires a detection system suited for time resolved X-ray spectroscopy [6]. The characteristic X-rays from muonic atoms formed in different targets were detected using HPGe detectors (orange in the drawing) and eight scintillating counters based on $LaBr_3(Ce)$ crystals (star-shaped structure, almond green in the drawing), whose outputs were recorded for 5 $\mu$s using a 500 MHz digitizer to measure both energy and time

spectrum of the recorded events. With a detailed pulse analysis, the expected characteristic X-rays and lifetimes of various elements present in the setup were measured. For this measurement the target was filled with a mixture of hydrogen and oxygen $H_2 + 0.3\%O_2$, measured by weight. The hydrogen gas contained a natural admixture of deuterium (135.8±0.1 ppm [7]). The target was thermalized using a Sumitomo helium cold head. In this case six temperatures were kept stable for three hours each, from 100 to 300 K degrees.

In this analysis, the characteristic X-rays of muonic atoms were detected using scintillating counters based on $LaBr_3$(Ce) crystals (energy resolution ≈3% at 662 keV and decay time $\tau = 16$ ns) read out by Hamamatsu R11265-200 PMTs. The acquired waveforms were processed off-line to reconstruct the time and energy of each detected X-ray.

Data taking was performed at the Riken muon facility of the Rutherford Appleton Laboratory (RAL), in Harwell (UK). Muons are produced in bunches with a repetition rate of 50 Hz. Each bunch is consisting of two spills separated by about 320 ns. Each spill can be roughly described as a gaussian distribution with FWHM of 70 ns and the starting muon momentum has a gaussian distribution with $\sigma_E/E \approx 10\%$ [8]. Beam users can tune the mean of the momentum distribution, which was chosen to be 57 MeV/c for the 2016 FAMU data taking.

Exiting the beam pipe collimator kapton window at a rate of about $10^5$ particle per second, muons crossed the FAMU beam hodoscope [9] and reached the aluminium vessel. They crossed a first external aluminium window, 0.8 mm thick, of the cryogenic container before entering the aluminium target window, 2.8 mm thick, which contained the gas. The gas mixture was prepared at 41 bar at 300 K. The thermal cycle was performed keeping a constant density.

## 3. Experimental method

The transfer rate measurement as function of the muonic hydrogen kinetic energy must be performed in a thermalized condition. In this state, the kinetic energy of the $\mu p$ follows a Maxwell-Boltzmann distribution at a given target temperature.

However, soon after the muon capture, the $\mu p$ atom gains kinetic energy due to its de-excitation. Data were taken with a gas density such as the thermalization of muonic hydrogen, following the muon capture, requires less than about 150 ns [10]. The 0.3% concentration (by weight) of $O_2$ used in the gas mixture, was chosen in order to have a mean transfer time greater than 150 ns. This allowed the system to be fully thermalized after few hundred nanoseconds from the arrival of the last muon. Under these conditions, the average kinetic energy of muonic hydrogen can be assumed as the Maxwellians corresponding to the gas temperature.

In the 2016 experimental setup, differently to the previous data set [6, 11], a persistent X-ray emission from muonic oxygen de-excitation was detected in the delayed phase, from 300 to about 5000 ns after the muon spill.

Hence, a study of the time evolution of the oxygen line emission can be performed to measure the transfer rate. Since the transfer process occurred in the delayed phase, in this analysis the large background of X-rays prompt emission from all the elements of the target - mostly aluminium, nickel, gold, and carbon - was strongly suppressed and it was negligible.

The variation of number of muonic hydrogen atoms $N_{\mu p}$ present in the target in the time interval $dt$ can be expressed by:

$$dN_{\mu p}(t) = S(t)dt - N_{\mu p}(t)\lambda_{dis}dt, \tag{1}$$

where $S(t)$ is the number of muonic hydrogen generated in the time interval $dt$, and $\lambda_{dis}$ is the total disappearance rate of the muonic hydrogen atoms:

$$\lambda_{dis} = \lambda_0 + \phi\,(c_p\Lambda_{pp\mu} + c_d\Lambda_{pd} + c_O\Lambda_{pO}). \tag{2}$$

Here $\lambda_0$ is the rate of disappearance of the muons bounded to proton (that includes both muon decay and nuclear capture), $\Lambda_{pp\mu}$ is the formation rate of the $pp\mu$ molecular ion in collision of $\mu p$

with a hydrogen nucleus, $\Lambda_{pd}$ denotes the muon transfer rate from $\mu p$ to deuterium, and $\Lambda_{pO}$ is the muon transfer rates from $\mu p$ to oxygen. The $pp\mu$ formation and muon transfer rates are all normalized to the liquid hydrogen number density (LHD) $N_0 = 4.25 \times 10^{22}$ cm$^{-3}$, and $\phi$ is the target gas number density in LHD units. The atomic concentrations of hydrogen, deuterium, and oxygen in the gas target, indicated by $c_p$, $c_d$, $c_O$, are related to the number densities of the latter, $N_p$, $N_d$, and $N_O$, by:

$$c_p = N_p/N_{tot} \ , \ c_d = N_d/N_{tot} \ , \ c_O = N_O/N_{tot} \ ,$$

$$N_{tot} = N_p + N_d + N_O \ , \ c_p + c_d + c_O = 1 \ .$$

The unknowns in equation 1 and 2 are therefore $S(t)$ and $\Lambda_{pO}$. In this analysis only the delayed phase is considered so, by definition of delayed phase, $S(t)$ is a constant term and from equation 1 it is possible to extract the transfer rate $\Lambda_{pO}$. Gas parameters depend on the composition, temperature, and pressure as described below; values were set as follows:

- filling was performed at $T = 300$ K, at a pressure $P = (41.00 \pm 0.25)$ bar, with $O_2$ concentration of $(0.30 \pm 0.09)\%$, mass weighted;
- the number densities of the gas mixtures are $\phi = (4.869 \pm 0.003) \times 10^{-2}$ in LHD atomic units, as derived from previous values;
- the atomic concentrations of oxygen $c_O = (1.9 \pm 0.3) \times 10^{-4}$ is derived from previous values; the deuteron concentrations $c_d = (1.358 \pm 0.001) \times 10^{-4}$ was obtained from a laboratory measurement [7];
- remaining data were taken from literature and theoretical calculations: $\Lambda_{pp\mu} = 2.01 \times 10^6$ s$^{-1}$ [12], $\Lambda_{pd} = 1.64 \times 10^{10}$ s$^{-1}$ as function of temperature [13], $\lambda_0 = (4665.01 \pm 0.14) \times 10^2$ s$^{-1}$ [12, 14].

A fit of the oxygen X-rays time evolution can be performed numerically integrating equation 1 by leaving $\Lambda_{pO}$ as free parameter.

## 4. Data analysis

The experimental sample, used in this work, consists of about $2.6 \times 10^6$ muon triggers (double spills), corresponding to $\approx 7.8 \times 10^7$ reconstructed X-rays coming from seven out of eight $LaBr_3$(Ce) detectors. One $LaBr_3$(Ce) detector output was not used in this analysis due to hardware problems. Target temperature was set at 100, 150, 200, 240, 273 and 300 K for three hours. A precise temperature measurement (relative error $\sigma_T/T$ better than $10^{-5}$) was performed using two probes and it was recorded together with the data at each trigger. Eleven temperature bins were chosen, six corresponding to the set temperatures and five corresponding to intermediate values with rapidly changing temperature. The time needed to the system to stabilize at a set temperature varied from half hour to about an hour and a half, depending on the set temperature and on external conditions.

To extract the transfer rate as function of the kinetic energy of the $\mu p$ atom, the following procedure was used:

1) $LaBr_3$(Ce) detectors were calibrated and their signals were integrated all together.
2) Good events were selected from the data set and selection efficiencies were evaluated.
3) The delayed events of each data set corresponding to a temperature bin were recorded into several time bins. For each time bin the energy spectrum in the range from 50 to 500 keV was obtained, in fact we considered the $K_\alpha(133 \text{ keV}), K_\beta(158 \text{ keV}), K_\gamma(167 \text{ keV})$ X-ray lines from oxygen when evaluating $\Lambda_{pO}$. For each energy spectrum, a background was evaluated and subtracted.

4) For each temperature the set of data was fitted, as explained in the previous section, obtaining a value for the transfer rate.
5) For every set of data corresponding at a given temperature bin, the mean kinetic energy of the $\mu p$ was evaluated.

Whenever needed, possible sources of systematical errors were investigated. Each item of this procedure is explained with more details in the following.

### *4.1. Detector calibrations*

Signals coming from the $LaBr_3(Ce)$ detectors were saved as waveforms by the acquisition system. A C++/ROOT based software was used to distinguish the pulses and to reconstruct their energy by fitting the waveform [5]. To each detected X-ray signal a time start and an energy in ADC channel was associated. The calibration from ADC channels to energy was performed independently for each detector using the data set itself.

Prompt and delayed X-ray lines were used first to correct for any fluctuation due to temperature variation inside the experimental hall. These were small long term variations of few keV in several hours due to the read-out electronics. This correction was needed to improve the overall energy resolution and to normalize the response of the behaviour of different detectors.

The ADC spectrum for each detector was converted to energy by comparing the position of the detected peaks to the known X-ray lines. We used a $\chi^2$ minimization algorithm on the energy region of interest. Calibration results are shown in figure 1, right panel, for the seven detectors used in this analysis. Each line color corresponds to a different detector. The energy spectra are not normalized. The different number of events detected depended on the detector position around the target. In fact, the overall cylindrical symmetry of the system was broken by the position of the insulating materials and of the copper braids used to thermalized the inner pressurized vessel. From the figure it can be noticed that the $K_\beta$ and $K_\gamma$ lines cannot be resolved, being the energy resolution of these detectors about 9% (FWHM) [5].

In this analysis, the energy spectra of the seven detectors were summed to increase the statistics.

### *4.2. Data selection and selection efficiencies*

Each trigger corresponded to an acquisition window of about 10 $\mu$s. Since the data analysis consists in the study of the time evolution of oxygen X-rays signals in this time window, each time-dependent effect was carefully studied and taken into account. In this experimental setup the delayed phase started at 1200 ns, about 300 ns after the arrival of the second muon pulse. We refer to events from time zero to 1200 ns as to "prompt" emission.

The reconstruction software read the waveform, recorded every 2 ns, in order to detect and process every single pulse. Pulse recognition was performed by setting a fixed threshold on the derivative of the waveform. The software was able to detect with very high efficiency X-rays with energy greater than few keV and separation greater than the signal rise time (12 ns). A realistic simulation of the waveform showed that the software recognized X-rays with energy greater than 20 keV and separation greater than 15 ns with an efficiency greater than 99.9%.

Once defined the start time of each pulse, the software performed a fit of the waveform in order to measure correctly the amplitude (i.e. the energy) of piled up signals. The number of piled up signals varied in the trigger window. Figure 2, panel on the top left, shows the counts of detected X-rays as function of the time. The two peaks correspond to the muon arrival time and they have the same profile of the muon beam, i.e. 70 ns FWHM and separation of 320 ns. The percentage of single pulses, as detected by the reconstruction software, is shown in the bottom left panel. In the delayed phase, the number of piled up events becomes soon

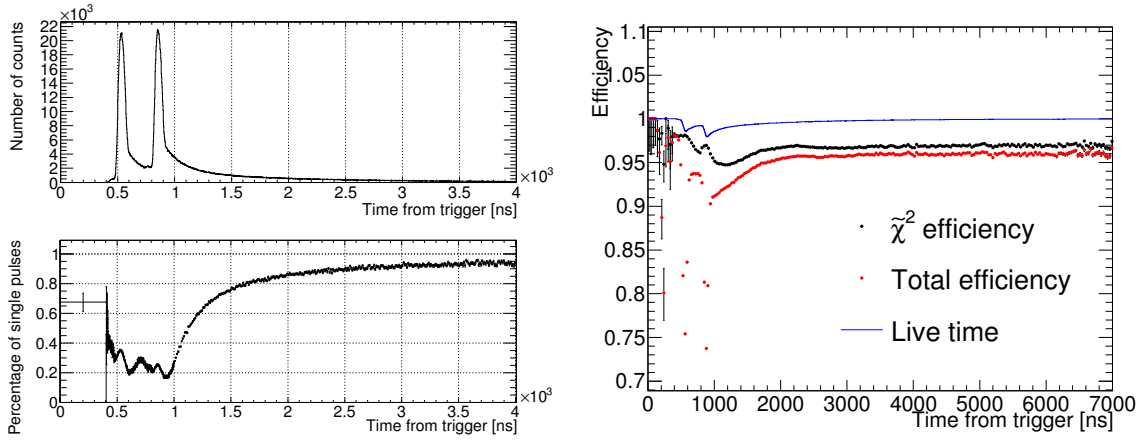


**Figure 2.** Top left panel: time distribution of X-rays reconstructed events. Bottom left panel: percentage of single pulses as function of time. Right panel: selection efficiencies (circles) and detector fractional live time (blue line).

very small. Consequently the probability of having piled up events with separation smaller than 12 ns ("perfect" pile up) was considered negligible.

Weak selection were applied on the reduced $\chi^2$ ($\tilde{\chi}^2$) coming from the fitting algorithm and on the signal separation. These selections were chosen in order to reject badly reconstructed events keeping as flat as possible the selection efficiency as function of time. Since the correlation between the start time and the fit result is weak, it was possible to estimate the selection efficiency using the data set itself - at least in the delayed phase where the reconstruction efficiency is close to the unity. Figure 2, on the right, shows the resulting $\tilde{\chi}^2 < 100$ selection efficiency as function of the time (black circles). The separation selection efficiency (distance between signals greater than 30 ns) was evaluated on the events passing the $\tilde{\chi}^2$ selection and it was close to 99% efficiency (not shown in figure). The overall efficiency was of about 96% and it was almost time independent in the delayed phase, red circles in figure 2 (left panel).

The last possible time dependent effect was the live time of the detectors. $LaBr_3(Ce)$ crystals and their electronics are very fast, however in this experiment their energy range was limited to about 800 keV by the number of channels of the digitizer. Signals with higher energy deposit saturate the ADC channels, giving a plateau on the waveform. The width of the plateau depended on the energy release. During this time the detector was not able to detect other signals, hence we defined these periods as "dead time". This dead time varied in the trigger window depending on the pile-up and on the type of particles hitting the detector (charged particles usually give a saturated signal). The live time and dead time was measured using the data themselves and an overall average correction was applied. Live time was measured for each detector independently and the live time correction was applied before summing the detectors signals. The $LaBr_3(Ce)$ detector were chosen for their fast response, consequently the live time is very high. An example of fractional live time for one detector and a subset of data is shown in figure 2, right panel blue line. Correction on the data was always less than 2%.

### *4.3. Background estimation*

Spectra of the selected data sample were corrected for all the found efficiencies and for the fractional live time. Then, the data were sampled into eleven temperature bins.

For each temperature bin the energy spectrum of delayed events was studied as function of

the time. The delayed time window from 1200 to 10000 ns was split into 20 bins. An example of

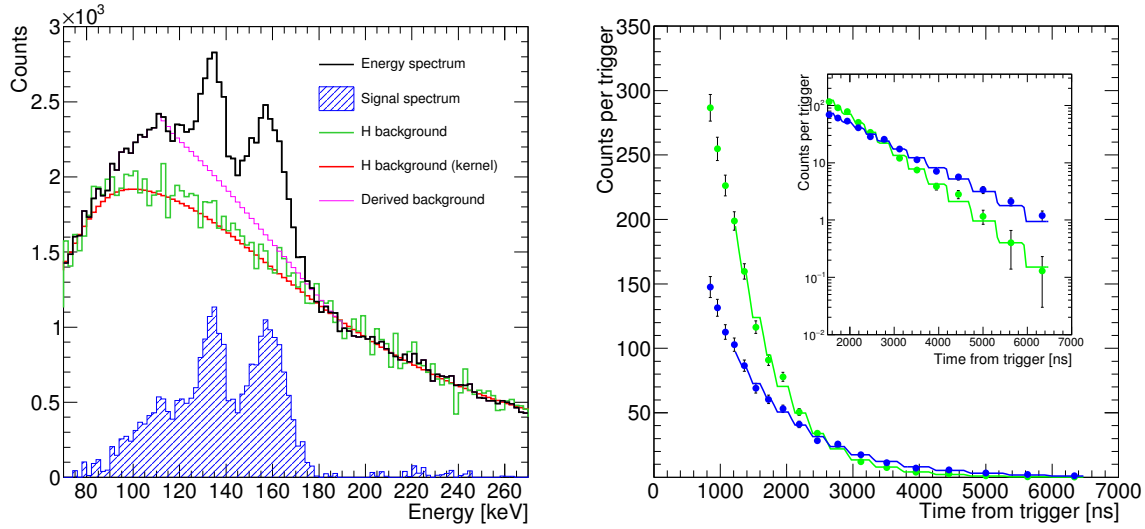


**Figure 3.** Left panel: example of energy spectrum signal in the time bin [1450,1650] ns at 300 K. Right panel: time dependence of the oxygen signal at 300 K (green points and line) and at 100 K (blue points and line). Lines are fit to the data. Error bars represent statistical and background-related systematics summed quadratically. Inset: zoom of the figure in logaritmic scale.

a delayed energy spectrum is shown in figure 3, black line in the left panel, at the temperature of 300 K and the time bin from 1450 to 1650 ns. The oxygen lines are seen over the background. The background estimation and subtraction for each time and temperature bin was the most subtle point of this work. Detector signals, in fact, showed a tail towards low energies due both to physics (Compton energy losses in the supporting material) and to electronics (most probably small gain variations due to the muon beam rate). Unfortunately, in the case of the oxygen mixture, the tail goes down to about 100 keV, where the energy spectrum naturally bend towards lower values. In such a situation it was impossible to estimate the background directly from the data. The background derived as an interpolation, or even more complex spectroscopic algorithms like the one provided by the ROOT class "TSpectrum" [15], gave an overestimated background (e.g. magenta line in figure 3, left panel). Better results were obtained using the spectrum detected with the target filled with pure hydrogen, at the same temperature and pressure. The hydrogen background is shown as a green line in figure. However, the acquired statistics with pure hydrogen was about one tenth of the gas mixture one. The low statistics in the background subtraction resulted in higher fluctuations on the signal data. In order to reduce these fluctuations the hydrogen data set was smoothed using a gaussian kernel algorithm [16], with smoothing parameter set to the energy resolution of the $LaBr_3(Ce)$ detectors. The result is shown as a red line in figure 3, on the left, and it was used to get the signal spectrum (hatched blue line histogram).

Fluctuations due to the normalization of the background and to the type of background subtraction (raw or with kernel smoothing method) were considered as systematic errors. This type of systematics was associated to each spectrum, i.e. each time bin of each temperature. The net result was a systematical fluctuation of the measured transfer rate around the true value, with no absolute trend. We compared backgrounds obtained with different methods and

parameters and the results obtained with different normalization regions for the background. These tests permitted us to estimate the effect of this systematic between 5% and 20% on the integrated signal spectrum (depending on the bin statistics). We decided to sum quadratically this systematic with the statistical error for each signal spectrum, before performing the fit to the data that provides the transfer rate measurement.

*4.4. Data fit and systematical uncertainties evaluation*

Time dependence for oxygen lines at the two temperature extremities – 300 K (green points) and at 100 K (blue points) – is shown in figure 3 (right panel). Each point represents the integrated signal after the background subtraction for each time bin. The fit was performed between 1200 ns, when the delayed phase started, and 6500 ns, when the signal was still detectable above the background. The fit to the data are shown as solid lines. The step-like behaviour is due to the numerical integration procedure used to calculate the function for each time bin. It can be noticed how the slope of the two distribution is significantly different, corresponding to different transfer rate measurements as function of the temperature.

As explained previously, the error bars associated to the points include both statistical and background-systematic errors summed quadratically.

Since the fit of the data was performed by numerically integrating equation 1, uncertainties on the equation parameters result in additional systematical uncertainties on the measured transfer rate. The estimation of systematical effects was done by varying the parameter values by the known errors. Systematic uncertainties were considered negligible whenever smaller than 1%.

The gas used to create the mixture were high purity gases, 99.9995% pure, corresponding to a contamination of other gases smaller than 5 ppm. The simulation proved that such a contamination imply negligible differences in the results. However, the gas mixture was prepared by the gas supplier by weight with a relative error of 3%. Propagation of this uncertainty in the fitting formula brings both different atomic concentrations and gas density. The overall effect on the final measurement is of the order of about 3%.

The gas filling procedure for this mixture was erroneously performed without a precise pressure reading. Consequently the uncertainty on the gas density had an effect on the transfer rate measurement of the order of about 3%.

All other items considered as possible source of systematics were proved to have negligible effects to the final measurement. These included the error (given in the literature) in the determination of the muon decay time (proton-bounded) $\lambda_0$; the literature error in the determination of transfer rate to $pp\mu$ molecule $\lambda_{pp\mu}$; the error in the determination of transfer rate to deuterium $\lambda_{pd}$; the error in the isotopic composition of hydrogen gas $c_d$.

Other consistency check were also performed on data by selecting separately $K_\alpha$ and $K_{\beta,\gamma}$ lines, by varying time fit window, and by applying much stricter selection criteria (e.g. $\tilde{\chi}^2 < 10$ and pulse time separation greater than 100 ns). All these checks resulted in a smaller data set and in a consequent statistical fluctuation around the higher statistics value.

*4.5. Temperature to kinetic energy conversion*

Given a fixed temperature, the conversion to kinetic energy can be performed by calculating the mean of a Maxwell–Boltzmann distribution. In our data set, however, the temperature slowly varied around a set value. The variation was due to the thermal capacitance of the target. To reduce the acquisition time and increase the statistics we decided to use the whole data set instead of waiting for a thermalization better than a given temperature threshold. Hence, for each trigger the target temperature was recorded and was associated to the detected X-rays.

Therefore, the measurement of the mean kinetic energy was obtained by the following procedure. For each X-ray passing the data selection and with energy inside the integrating region (both signal and background events) a Maxwellian function was calculated. The

Maxwellian functions of all the triggers recorded at a given temperature bin were summed. The mean of the resulting distribution was chosen as a measurement of the kinetic energy. Final results will be presented as function of the measured kinetic energy.

## 5. Results

Preliminary transfer rate results are shown, as function of the temperature, in figure 4. This

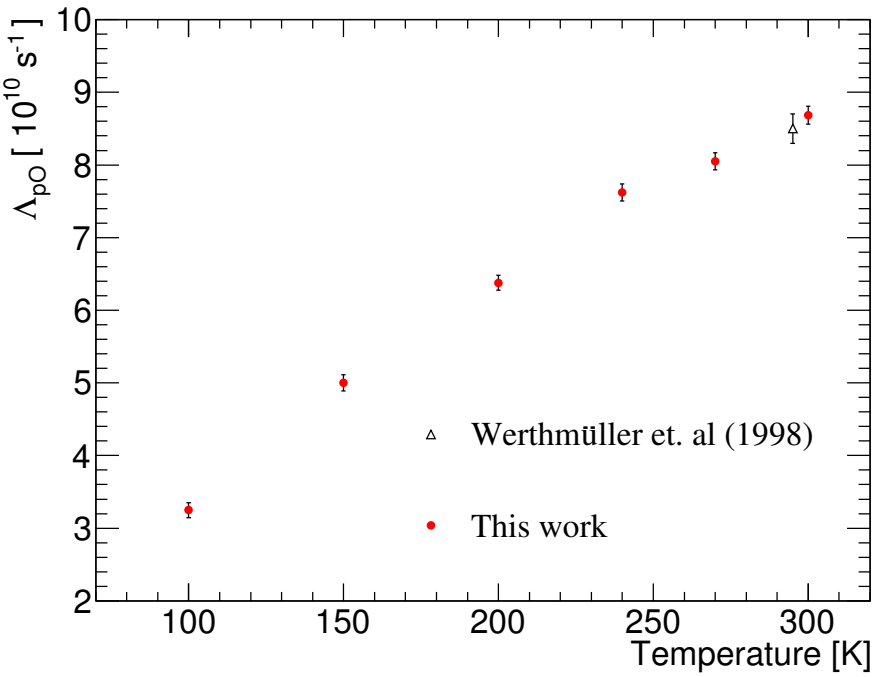


**Figure 4.** Transfer rate measurement as function of the temperature. The result obtained by Werthmüller et al. at PSI at 294 K [17] is also shown.

is the first precise measurement of the temperature dependence of transfer rate from muonic hydrogen to oxygen. Our results are in excellent agreement with the previous measurement at 294 K [17]. Error bars represent the error on the fit result obtained as described in previous section, i.e. errors include statistical and background-related systematics. Other systematics are not included.

## 6. Conclusions

The experimental results described here represent a fundamental step in the development of the FAMU project.

Data were taken in 2016 with a dedicated cryogenic thermalized gas target and with optimal concentrations. The confirmation of the theoretically predicted temperature dependence of the transfer rate from muonic hydrogen to oxygen will permit to proceed with the measurement of the muonic hydrogen ground state hyperfine splitting. Moreover, this precise measurement will allow to optimize the target and detection system for the final experiment.

Other elements gas mixtures data taken in the same run are under study and results will be the topic of future publications.

**Acknowledgments**
The research activity presented in this paper has been carried out in the framework of the FAMU experiment funded by Istituto Nazionale di Fisica Nucleare (INFN). The use of the low energy muons beam has been allowed by the RIKEN RAL Muon Facility. We thank the RAL staff (cooling, gas, and radioactive sources sections) and especially Mr. Chris Goodway, Pressure and Furnace Section Leader, for their help, suggestions, professionalism and precious collaboration in the set up of the experiment at RIKEN-RAL.

We gratefully recognize the help of T. Schneider, CERN EP division, for his help in the optical cutting of the scintillating fibers of the hodoscope detector and linked issues and N. Serra from Advansid srl for useful discussions on SiPM problematics.

We thank our colleagues Chiara Boschi and Ilaria Baneschi (IGG, CNR Pisa) for their help in the measurement of the gas isotopic composition.

A. Adamczak and D. Bakalov acknowledge the support within the bilateral agreement between the Bulgarian Academy of Sciences and the Polish Academy of Sciences. D. Bakalov, P. Danev and M. Stoilov acknowledge the support of Grant 08-17 of the Bulgarian Science Fund.

[1] Pohl R *et al.* 2010 *Nature* **466** p 2010
[2] Gershtein S S 1958 *J. Exptl. Theoret. Phys.* **34** p 318
[3] Werthmüller A *et al.* 1996 *Hyp. Interact.* **103** p 147
[4] Mukhopadhyay N C 1977 *Phys. Rep.* **30** p 1
[5] FAMU collaboration 2018 *The layout of the FAMU (R582) experiment at RAL to study the muon transfer rate from hydrogen to other gases in the epithermal range* to be submitted to JINST
[6] Adamczak A *et al.* 2016 *J. of Inst.* **11** p P05007
[7] Boschi C and Baneschi I 2016 CNR Internal Report (unpublished)
[8] Matsuzaki T *et al.* 2001 *Nucl. Instr. Meth.* A **465** p 365
[9] Bonesini M *et al.* 2017 *J. of Inst.* **12** p C03035
[10] Bakalov D *et al.* 2015 *Phys. Lett.* A **379** p 151
[11] Mocchiutti E *et al.* 2018 *J. of Inst.* **13** p P02019
[12] Andreev A *et al.* 2015 *Phys. Rev.* C **91** p 055502
[13] Chiccoli C *et al.* 1992 *Muon Catal. Fusion* **7** p 87
[14] Suzuki T, Measday D F and Roalsvig J P 1987 *Phys. Rev.* C **35** p 2212
[15] Morhac M *et al.* 2000 *Nucl. Instr. Meth.* A **443** p 108
[16] Hastie T, Tibshirani R and Friedman J 2001 *The Elements of Statistical Learning* (Springer) ISBN 0-387-95284-5
[17] Werthmüller A *et al.* 1998 *Hyp. Interact.* **116** p 1